Sharp three-dimensional notches under combined nominal normal and shear fatigue loading

M. Vormwald, E. Shams
Technische Universität Darmstadt, Department of Civil and Environmental Engineering, Materials Mechanics Group, Franziska-Braun-Str. 3, 64287 Darmstadt, Germany
vormwald@wm.tu-darmstadt.de, shams@wm.tu-darmstadt.de

ABSTRACT. Many engineering structures are exposed to non-proportional fatigue loading. However, at the critical location of crack initiation, often only one of the load sequences dominates – the individual load cases result in different crack initiation sites. Based on engineering judgment a simplified local uniaxial or proportional loading situation may be assessed. In general, the critical location must be identified by calculating fatigue lives for a variety of locations. The position of the critical location depends on the hypothesis applied for life calculation – besides loading, geometry, material and many other influence factors. For sharp three-dimensional notches the region for the search of the critical location may be restricted considerably. Weld start and stop points are an industrial example for such sharp notches. They are the object of the present investigation. They are exposed to nominal normal and shear loading. The individual hot spots for crack initiation lie necessarily close together. A strong interaction of the loading cases for both proportional and non-proportional loading was experimentally observed. In the numerical investigation notch stresses were calculated using an idealised weld end model. Based on the critical plane approach according to Findley, numerical interaction lines were produced.

KEYWORDS. Combined loading; Multiaxial fatigue; Notch stress concept; Critical plane appraoch; Weld ends.

OPEN ACCESS

Citation: Vormwald, M., Shams, E., Sharp three-dimensional notches under combined nominal normal and shear fatigue loading, Frattura ed Integrità Strutturale, 41 (2017) 114-122.

Received: 28.02.2017
Accepted: 15.04.2017
Published: 01.07.2017

Copyright: © 2017 This is an open access article under the terms of the CC-BY 4.0, which permits unrestricted use, distribution, and reproduction in any medium, provided the original author and source are credited.

INTRODUCTION

Welded structures often contain weld start and end points, which are the critical location for the failure. Normally, fatigue design of welded components proceeds from *S–N* curves (fatigue strength versus number of cycles). Concerning weld start and end points, the knowledge of *S-N* curve parameters is limited to either normal [1-5] or shear [6] stressed structures. In these investigations, dealing only with uniaxial loading conditions, geometrically idealised weld end models with concept radii of r_{normal} = 0.20 mm respectively r_{shear} = 0.05 mm were created.

These models base on the real weld geometry obtained by means of high-precision 3D-scanner. In connection with these models, recommendations for determining notch stresses by applying the finite element (FE) method were developed. Nowadays, different *S-N* curves are assigned to weld toe and weld root failure scenarios induced by normal and shear stresses. For the case of failure at weld root, a fatigue assessment concept covering both geometrical and statistical size effects was presented in [7].
Many research activities have been initiated during the last years for the investigation of fatigue design of multiaxially loaded welded joints [8-10]. Nevertheless, the case of weld ends under such loading is not sufficiently explored yet.
In the present paper, the fatigue behaviour of weld ends under combined in- and out-of-phase multiaxial loading in thin sheet structures, which is of special interest in the automotive industry, is addressed. In the experimental part of this research, cycles to failure at different stress amplitudes were derived from fatigue testing. Due to the complex geometry of weld ends, the notch stress concept was used in order to assess the multiaxial stress-states based on an idealised weld end model. The critical plane oriented criteria according to Findley [11] has been applied, in order to determine interaction lines for proportional and non-proportional loading cases.

EXPERIMENTAL INVESTIGATION

Specimens and Testing

Fatigue tests were conducted on welded tube-tube joints from fine-grained and engineering steels (outer tube: S340+N and inner tube: E355+N) under constant amplitude loading in the range of 10^4 to $5 \cdot 10^6$ cycles to failure. The 490 mm-long test specimen consists of two tubes with an overlap length of 60 mm. The external diameters of the inner and outer tubes are $d_{a,1}$ = 40 mm and $d_{a,2}$ = 45 mm, respectively. The inner tube has a sheet thickness of t_1 = 2.0 mm; the sheet thickness of the outer tube is t_2 = 2.5 mm. Two seam welds at opposing quadrants joined the two tubes, see Fig. 1. The tube-tube joints were manufactured using gas shielded metal arc welding. The welding was carried out in a twin-robot system, where two robots work simultaneously.

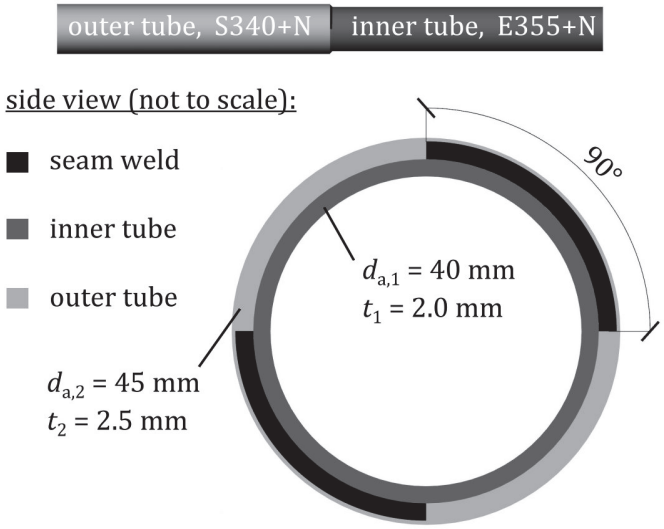

Figure 1: Overlapped tube-tube specimen.

The fatigue test program shown in Tab. 1 was carried out. The specimens were subjected to alternating pure axial force, pure torsional moment and proportional as well as non-proportional combinations of both loadings. In the latter case the phase shift was set at 90°. In the case of combined loading two ratios were considered for the torsional moment to the axial force amplitudes $M_{T,a}$ / $F_{\perp,a}$. This ratio was set to 28 Nm / kN on the one hand and 17.9 Nm / kN on the other hand, see series 01-06 in Tab. 1. Herein, dimensionless ratios expressed by nominal stress amplitudes τ_a / σ_a are also given. In series 01-06 any effect on residual welding stresses is excluded because all the specimens were stress-relieved by heat treatment (600°C for 6 hours and followed by slow cooling) prior to testing. Furthermore, four test series (series 07-

10) were scheduled for specimens not exposed to any heat treatment in an as-welded condition in order to investigate the influence of residual stresses on fatigue resistance.
The experiments have been conducted using a servo-hydraulic multi-axial test rig with testing frequencies of 8-10 Hz for uni-axial and 1-2 Hz for multi-axial loading conditions. The experimental set-up is depicted in Fig. 2. Prior to testing the specimens were sprayed using a scan spray in order to ease the optical detectability of both formation and growth of fatigue cracks after the test. In Fig. 2a scan of the specimen in the sprayed welded area comprising start (left) and end points (right) is shown. During testing, the fatigue cracks were monitored by taking photographs of the four existing weld start and end points at predefined numbers of cycles. If predefined upper and lower limits for deformation values were exceeded, the experiment was terminated. The limits for deformation values were set to ±8 mm and ±5 degrees. The corresponding number of cycles is defined as the failure criterion.

series	condition	R	$F_\perp$	M_T	$M_{T,a}$ / $F_{\perp,a}$ in Nm/kN	τ_a / σ_a	δ	number of specimens
01	stress-relieved	-1	+	-	-	-	-	7
02	stress-relieved	-1	-	+	-	-	-	7
03	stress-relieved	-1	+	+	28.0	1.40	0°	7
04	stress-relieved	-1	+	+	17.9	0.895	0°	7
05	stress-relieved	-1	+	+	28.0	1.40	90°	7
06	stress-relieved	-1	+	+	17.9	0.895	90°	7
07	as-welded	-1	+	-	-	-	-	7
08	as-welded	-1	-	+	-	-	-	7
09	as-welded	-1	+	+	28.0	1.40	0°	7
10	as-welded	-1	+	+	28.0	1.40	90°	7

Table 1: Test program.

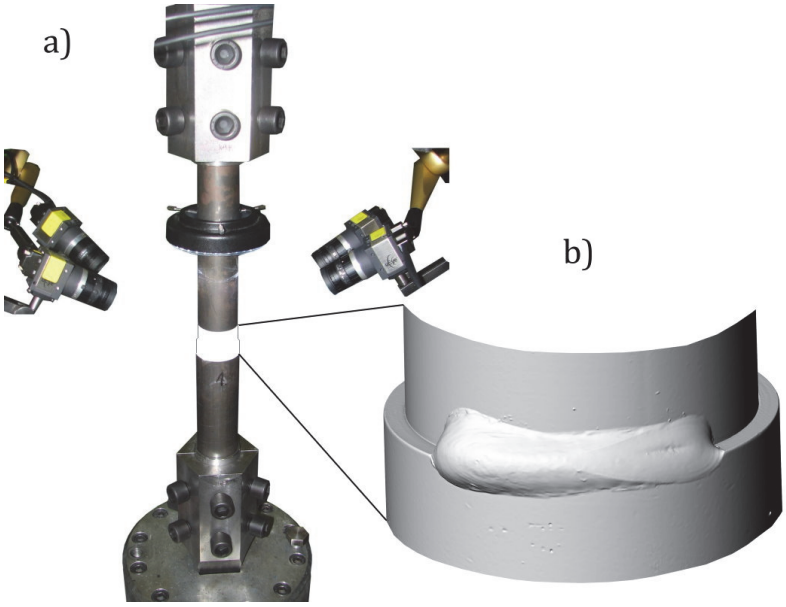

Figure 2: Experimental set-up a), scan of the weld b).

Results

Typical failures of specimens under pulsating uni-axial and multi-axial loading are shown in Fig. 3. Fatigue cracks initiated at the transition area between weld toe and root in all the tested specimens, either at the weld start or at the weld end

position. In the case of specimens under pure axial loading, the fatigue cracks were initiated in both the weld start and end locations. The crack fronts spread toward each other at the weld toe on the outer tube side during cyclic loading and finally coalesced into one crack, Fig. 3a. In specimens subjected to torsional moment the cracks spread to the inner and outer tube halves, Fig. 3b. In the case of combined in-phase loading the fatigue cracks spread either into the outer pipe or through the weld metal, Fig. 3c. In contrast, the welds failed only with crack spreading through the weld metal when force and moment were phase shifted by 90°, Fig. 3d.
The majority of fatigue life is spent during crack growth. A modelling of this mechanism is currently far behind numerical feasibilities, especially for the non-proportional loading cases [12]. Therefore, an approach based on notch stresses is applied as described in the next section.

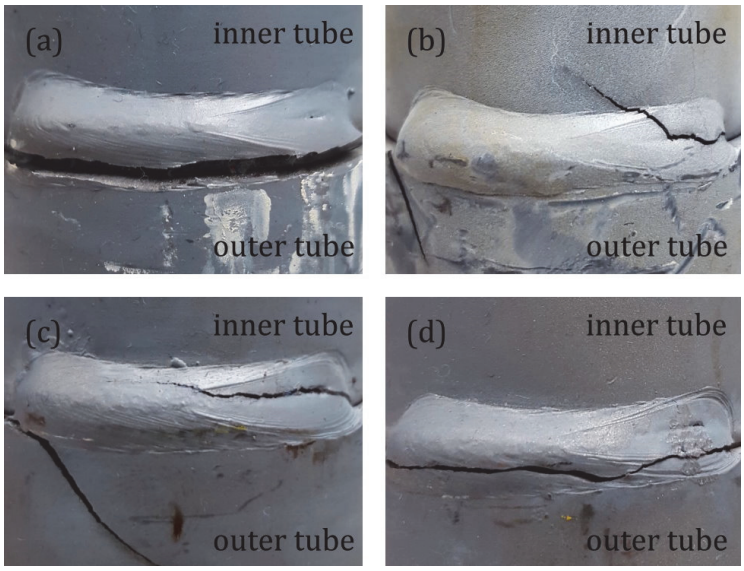

Figure 3: Failure modes of welded joints under axial force a), torsional moment b) and proportional c) as well as non-proportional d) combinations, R =-1.

The results are presented in form of *S-N* curves (nominal stresses versus number of cycles to failure) for stress-relieved specimens under alternating loading, Fig. 4, and also for as-welded specimens under alternating loading, Fig. 5. In each case, we have plotted normal stress amplitude (Figs. 4a and 5a), resulting from the axial force amplitude and shear stress amplitude (Figs. 4b and 5b), and from the torsional moment amplitude. A result was shown as run-out, when no cracks could be detected after $1 \cdot 10^6$ load cycles in the case of combined loadings or after $2 \cdot 10^6$ load cycles otherwise, symbols with horizontal arrows in Fig. 5. After such a test, the applied load(s) was/were doubled and the test was repeated, symbols with slanted arrows in Fig. 5. Regression lines are added for a 50% probability of survival. The slopes of the *S-N* curves, when described by a power law, vary within the range of 3.7 to 5.9 for stress-relieved specimens. The slopes of *S-N* curves are higher and vary between $6.1 \leq k \leq 7.7$ for specimens not exposed to any heat treatment.
The specimens in an as-welded state provide higher fatigue strengths as compared to stress-relieved specimens, especially in the area of higher fatigue lives. This indicates the existence of compressive residual stresses resulting from the welding process.

Interaction lines

Interaction diagrams make it possible to compare the experimental results shown as *S-N* curves among each other. Contours for constant fatigue lives can be plotted in a $M_{T,a}$-$F_{\perp,a}$ (or τ_a-σ_a) diagram. Also the phase shift for each contour is constant. In this way it is also possible to compare the experimental results as well as the out-of-phase behaviour. Indeed, the form of these contours is dependent upon fatigue life. An exceptional situation exists when the *S-N* curves all have the same slope. In this case, the form of the interaction lines is independent of the selected fatigue life. Fig. 6 shows the interaction lines in a $M_{T,a}$-$F_{\perp,a}$ diagram corresponding to $N_f = 10^5$. The dashed lines representing the results on non-proportional loadings always lie below the solid lines for proportional loadings.

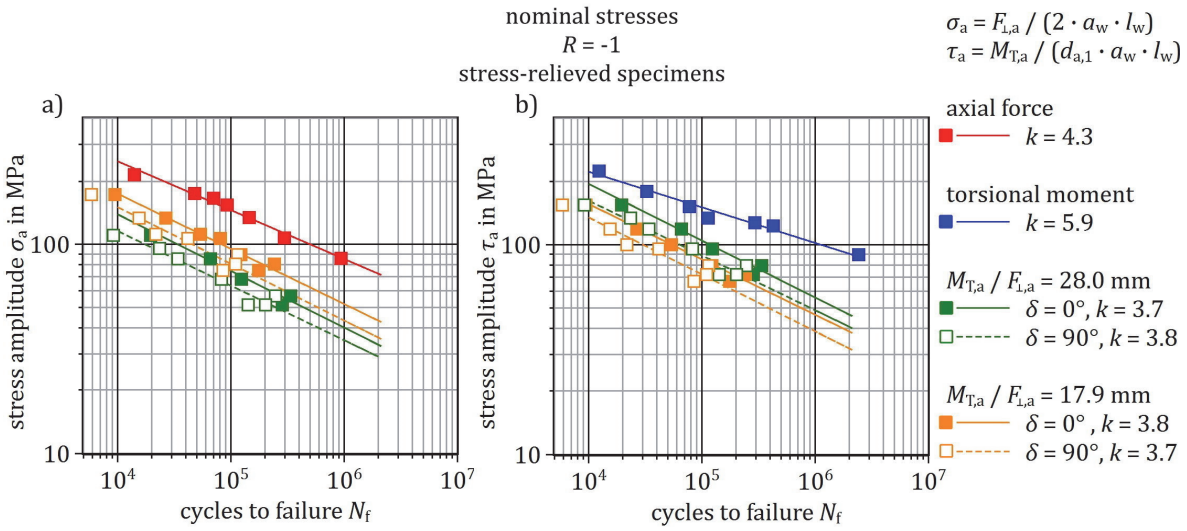

Figure 4: *S-N* curves for alternating loading and stress-relieved specimens.

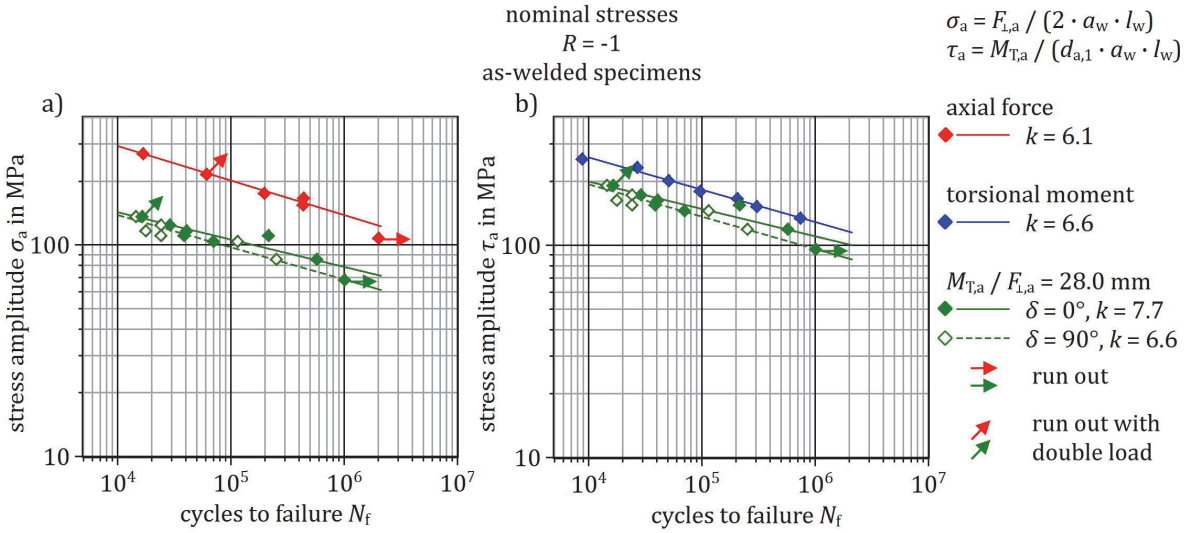

Figure 5: *S-N* curves for alternating loading and as-welded specimens.

NUMERICAL ANALYSES

Notch stresses

In the numerical part of the study, notch stresses were calculated with an idealised weld end geometry. The modelling steps of such an idealised weld end geometry are comprehensively described in [1-6]. A submodelling technique has been used, in order to calculate the von Mises equivalent stresses. The geometry of the submodel takes as a basis a radius of r_{root} = 0.05 mm at the weld root and a radius of r_{toe} = 0.2 mm at the weld toe, Fig. 7a. The solid FE-model, as shown in Fig. 7b, is represented as a mesh of tetrahedral elements with a quadratic shape function. It incorporates linear elastic material behaviour.

The maximum equivalent stresses were obtained for both cases in a zone, where weld root migrates to the weld toe at the weld end. This critical zone, which is not to be seen in the view of Fig. 7, consists of a part of cylindrical weld root and weld toe regions at inner and outer tubes. The local stresses are plotted in the critical zone for both load cases, see Fig. 8. The Figures indicate that in these cases the highly stressed nodes are located at completely different sites.

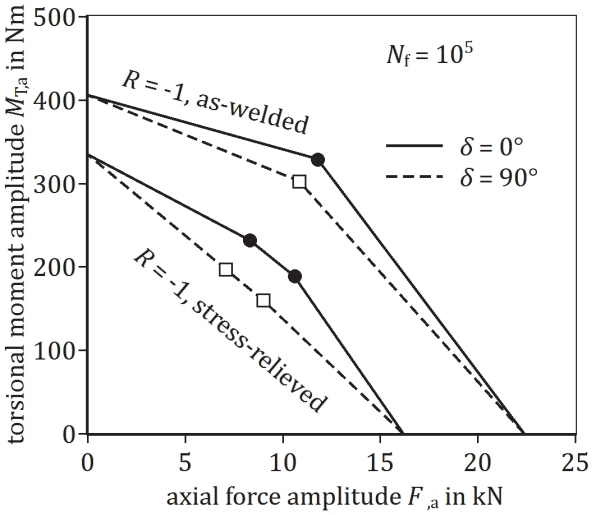

Figure 6: Interaction lines for $N_f = 10^5$.

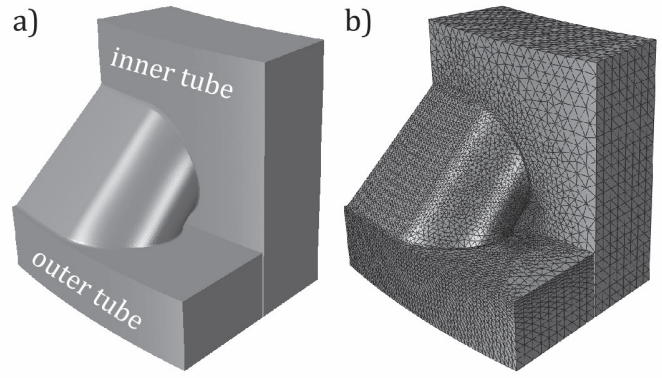

Figure 7: Geometry of the submodel a), FE-model b).

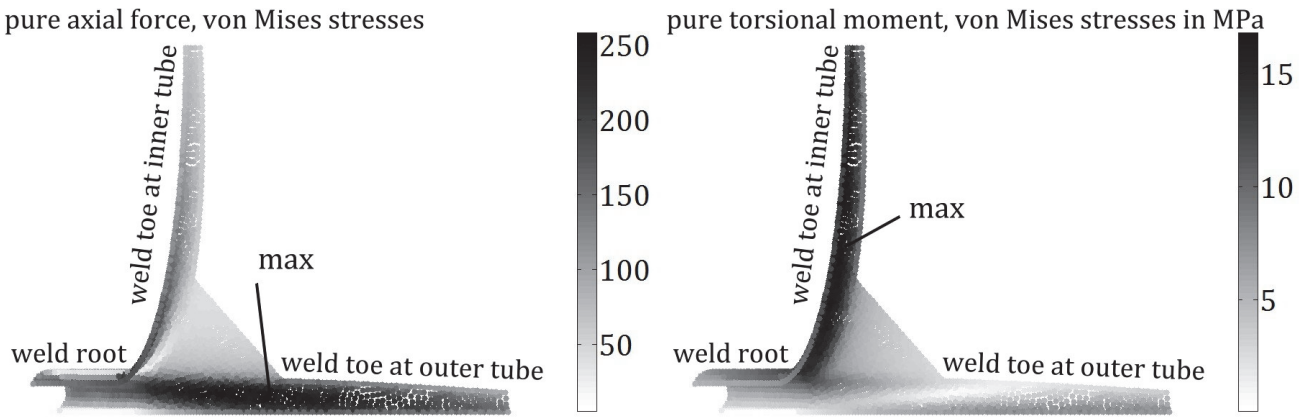

Figure 8: left: von Mises stresses at weld ends under pure axial force, right: von Mises stresses at weld ends under pure torsional moment.

Critical plane approach

Fatigue cracks originate normally from an unloaded surface of a structure. At the critical location, a plane stress condition can be assumed. For this case, the calculation of the stress components in arbitrary cutting planes is simplified, see Fig. 9. A cutting plane within a material is designated as a critical plane, if it leads to a maximal value of a specific damage

parameter. According to the Findley criterion [11], the critical plane has to be searched depending on both the shear stress range $\Delta\tau$ and maximal value of the normal stress $\sigma_{\gamma\varphi,\max}$, see Fig. 10. The parameter k in the given formula is a material parameter and was set to 0.2 for steel structures.

FE-calculations were performed for different moment-to-force ratios. For each node at the critical surface, see Fig. 8, three stress components, σ_{xx}, σ_{yy} and τ_{xy} were determined. The angles φ and γ were varied at each node, in order to determine the maximum value of the damage parameter f at the critical surface. The resulting interaction lines for proportional and non-proportional loading cases are depicted in Fig. 11. Such purely numerically obtained interaction lines can be assessed only in their shapes. Therefore, the axial force and torsional moment amplitudes were normalised using the pure axial force and pure torsional moment results.

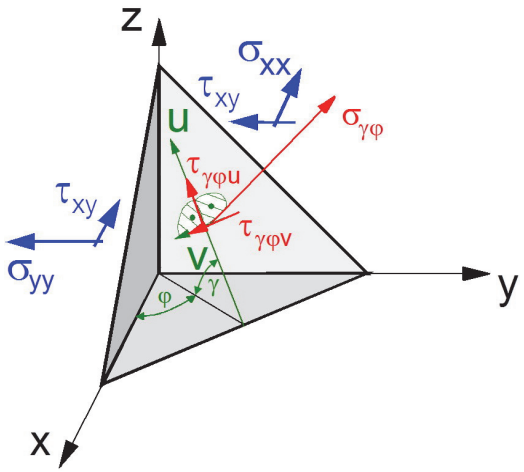

$$\sigma_{\gamma\varphi} = \sin^2\gamma\cdot\left[\frac{\left(\sigma_{xx}+\sigma_{yy}\right)}{2}+\frac{\left(\sigma_{xx}+\sigma_{yy}\right)}{2}\cos 2\varphi+\tau_{xy}\sin 2\varphi\right]$$

$$\tau_{\gamma\varphi} = \sqrt{\tau_{\gamma\varphi u}^2+\tau_{\gamma\varphi v}^2}$$

$$\tau_{\gamma\varphi u} = -\sin\gamma\cdot\left[\frac{\left(\sigma_{xx}-\sigma_{yy}\right)}{2}\sin 2\varphi-\tau_{xy}\cos 2\varphi\right]$$

$$\tau_{\gamma\varphi v} = -\sin\gamma\cdot\cos(\gamma)\cdot\left[\frac{\left(\sigma_{xx}+\sigma_{yy}\right)}{2}+\frac{\left(\sigma_{xx}-\sigma_{yy}\right)}{2}\cos 2\varphi+\tau_{xy}\sin 2\varphi\right]$$

Figure 9: Illustration of the stress components $\sigma_{\gamma\varphi}$, $\tau_{\gamma\varphi u}$ and $\tau_{\gamma\varphi v}$

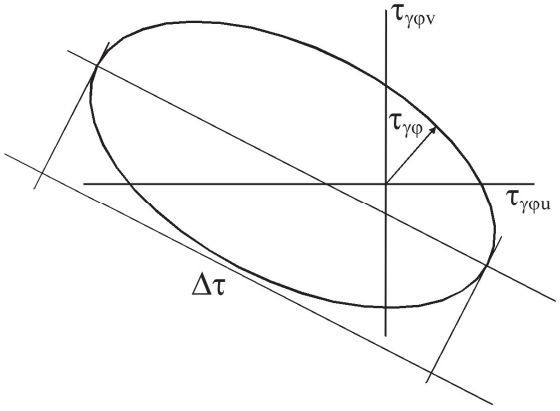

Findley parameter f:

$$\left(\frac{\Delta\tau}{2}+k\cdot\sigma_{\gamma\varphi,\max}\right)_{\max} = f$$

Figure 10: Determination of the shear stress range $\Delta\tau$ and Findley parameter f.

Conclusions

In all the tested specimens, fatigue cracks were initiated at the transition zone between weld toe and weld root. Using an idealised weld end model, the critical surface was rounded by $r = 0.05$ mm, in order to calculate equivalent stresses at the failure-critical location. The critical plane approach according to Findley was used, in order to determine interaction lines for proportional and non-proportional loading. In the case of non-proportional loading the interaction lines reveal a nearly complete decoupling. This result is in contrast of the experimental finding, especially for the non-

proportional loading cases. The reason for this discrepancy is only to a minor extent due to the applied criterion according to Findley. In [13] it is shown that also other criteria fail to explain the experimental results. The decoupling of the loading cases is mainly attributed to the local decoupling of the sites of maximum stresses in the 3D-notch, Fig. 8. For an improvement of prediction accuracy either the geometry model of the general assessment approach must be revisited.

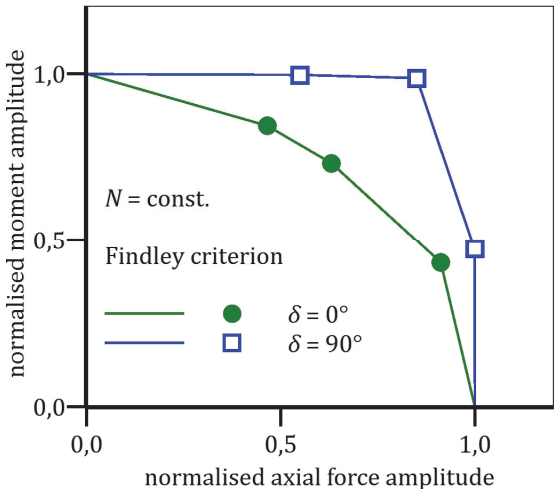

Figure 11: Normalised interaction lines for N = const.

ACKNOWLEDGEMENTS

The authors gratefully acknowledge the financial support of the research Project A 288 by the "Research Association for the Iron and Metalworking Industry e. V." (AVIF) and the "Foundation Research on Steel Application". Technical support during the project was given by the Research Association of Automotive Technology FAT. The specimens were provided by "Benteler Automobiltechnik GmbH" and the support is highly appreciated.

REFERENCES

[1] Kaffenberger, M., Vormwald, M., Application of the notch stress concept to the real geometry of weld end points, Mat.-wiss. u. Werkstofftech., 42 (2011) 289-297.
[2] Kaffenberger, M., Vormwald, M., Fatigue resistance of weld ends - Analysis of the notch stress using real geometry, Mat.-wiss. u. Werkstofftech., 42 (2011) 874-880.
[3] Kaffenberger, M., Malikoutsakis, M., Savaidis, G., Vormwald, M., Fatigue resistance of weld ends, Comput. Mater. Sci., 52 (2012) 287-292.
[4] Kaffenberger, M., Vormwald, M., Considering size effects in the notch stress concept for fatigue assessment of welded joints, Comput. Mater. Sci., 64 (2012) 71-78.
[5] Kaffenberger, M., Vormwald, M., Schwingfestigkeit von Schweissnahtenden und Übertragbarkeit von Schweissverbindungswöhlerlinien, Mater. Test., 55 (2013) 553-560.
[6] Shams, E., Malikoutsakis, M., Savaidis, G., Vormwald, M., Notch stress and fracture mechanics based assessment of fatigue of seam weld ends under shear loading, Fatigue Fract. Eng. Mater. Struct., 37 (2014) 740-750.
[7] Shams, Vormwald, M., Fatigue of weld ends under combined in- and out-of-phase multiaxial loading, Frattura ed Integrità Strutturale, 38 (2016) 114-120.
[8] Sonsino, C.M., Multiaxial fatigue of welded joints under in-phase and out-of-phase local strains and stresses, Int. J. Fatigue, 17 (1995) 55-70.
[9] Eibl, M., Sonsino, C.M., Kaufmann, H., Zhang, G., Fatigue assessment of laser welded thin sheet aluminium, Int. J. Fatigue, 25 (2003) 719-731.

[10] Wiebesiek, J., Störzel, K., Bruder, T., Kaufmann, H., Multiaxial fatigue behaviour of laserbeam-welded thin steel and aluminium sheets under proportional and non-proportional combined loading, Int. J. Fatigue, 33 (2011) 992-1005.
[11] Findley, W.N., A theory for the effect of mean stress on fatigue of metals under combined torsion and axial load or bending, J. Engng. Ind. (ASME) 81 (1959), 301–306.
[12] Zerres, P., Vormwald, M., Review of fatigue crack growth under non-proportional mixed-mode loading, Int. J. Fatigue, 58 (2014) 75-83.
[13] Shams, E., Vormwald, M., Fatigue of weld ends under combined loading, Int. J. Fatigue (2017), in press, DOI: 10.1016/j.ijfatigue.2016.12.020.